

Exotic states of bouncing and walking droplets

Øistein Wind-Willassen, Jan Moláček, Daniel M. Harris, and John W. M. Bush

Citation: *Phys. Fluids* **25**, 082002 (2013); doi: 10.1063/1.4817612

View online: <http://dx.doi.org/10.1063/1.4817612>

View Table of Contents: <http://pof.aip.org/resource/1/PHFLE6/v25/i8>

Published by the [AIP Publishing LLC](#).

Additional information on Phys. Fluids

Journal Homepage: <http://pof.aip.org/>

Journal Information: http://pof.aip.org/about/about_the_journal

Top downloads: http://pof.aip.org/features/most_downloaded

Information for Authors: <http://pof.aip.org/authors>

ADVERTISEMENT



Running in Circles Looking for the Best Science Job?

Search hundreds of exciting
new jobs each month!

<http://careers.physicstoday.org/jobs>

physicstodayJOBS



Exotic states of bouncing and walking droplets

Øistein Wind-Willassen,¹ Jan Moláček,² Daniel M. Harris,²
and John W. M. Bush^{2, a)}

¹*Department of Applied Mathematics and Computer Science, Technical University of Denmark, 2800 Kongens Lyngby, Denmark*

²*Department of Mathematics, Massachusetts Institute of Technology, 77 Massachusetts Avenue, Cambridge, Massachusetts 02139, USA*

(Received 20 March 2013; accepted 14 July 2013; published online 13 August 2013)

We present the results of an integrated experimental and theoretical investigation of droplets bouncing on a vibrating fluid bath. A comprehensive series of experiments provides the most detailed characterisation to date of the system's dependence on fluid properties, droplet size, and vibrational forcing. A number of new bouncing and walking states are reported, including complex periodic and aperiodic motions. Particular attention is given to the first characterisation of the different gaits arising within the walking regime. In addition to complex periodic walkers and limping droplets, we highlight a previously unreported mixed state, in which the droplet switches periodically between two distinct walking modes. Our experiments are complemented by a theoretical study based on our previous developments [J. Molacek and J. W. M. Bush, *J. Fluid Mech.* **727**, 582–611 (2013); **727**, 612–647 (2013)], which provide a basis for rationalising all observed bouncing and walking states.
© 2013 AIP Publishing LLC. [<http://dx.doi.org/10.1063/1.4817612>]

I. INTRODUCTION

Drops bouncing on a vibrating fluid bath^{1,2} have recently received considerable attention for two principal reasons. First, they represent a rich dynamical system, exhibiting many features of low-dimensional chaotic oscillators.^{3–5} Second, in certain parameter regimes, the bouncers walk horizontally through resonant interaction with their wave field.^{6–10} The resulting walkers represent the first known example of a macroscopic pilot-wave system,^{11–13} and exhibit many features thought to be exclusive to the microscopic quantum realm,¹⁴ including self-organising lattice structures,^{15,16} single particle diffraction,¹⁷ quantized orbits,¹⁸ orbital level splitting,¹⁹ tunneling effects,²⁰ and wave-like statistics in confined geometries.²¹

Consider a fluid of density ρ , kinematic viscosity ν , and surface tension σ in a horizontal bath of depth H driven by a vertical vibration of amplitude A and frequency $f = \omega/(2\pi)$. The effective gravity in the vibrating bath frame of reference is $g^*(t) = g + \gamma \sin(2\pi ft)$, where g is the gravitational acceleration and $\gamma = A\omega^2$. At low forcing acceleration, the fluid remains quiescent in the vibrating frame; however, above a critical acceleration amplitude γ_F corresponding to the Faraday threshold, the layer becomes unstable to a field of standing Faraday waves.^{22,23} The waves are subharmonic, with half the frequency of the vibrational forcing, $\omega_F = \omega/2$, and with wavelength $\lambda_F = 2\pi/k_F$ prescribed by the standard surface wave dispersion relation:

$$\omega_F^2 = \tanh(k_F H) \left(g k_F + \frac{\sigma k_F^3}{\rho} \right). \quad (1)$$

In the experiments of interest, the vibrational forcing is less than the Faraday threshold, $\gamma < \gamma_F$; consequently, the interface would remain flat if not for the presence of a droplet.

^{a)}bush@math.mit.edu

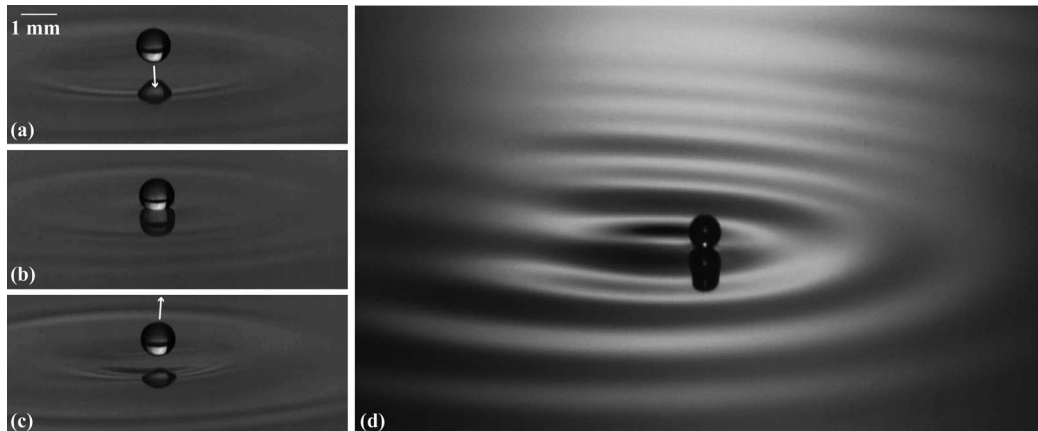


FIG. 1. Walking drop of 20 cS silicone oil of radius 0.48 mm (a) before, (b) during, and (c) after an impact with a bath of the same liquid vibrating at 70 Hz. (d) A walking drop and its associated wave field.

When a fluid drop is placed on a vibrating bath (Fig. 1), there are three basic outcomes: the droplet may either coalesce, bounce in place, or walk across the fluid surface.^{1,7,9} For $\gamma < \gamma_B$, where γ_B is the bouncing threshold, the applied forcing is insufficient to levitate the drop, which then settles towards the bath. The intervening air layer thins until reaching a critical thickness at which Van der Waals forces between drop and bath initiate coalescence. For $\gamma > \gamma_B$, this air layer is sustained during impact, precluding coalescence and enabling a stable bouncing state. Beyond a critical forcing threshold, $\gamma > \gamma_w$, where γ_w is the walking threshold, the stationary bouncing state is destabilised by the underlying wave field, giving way to a dynamic state in which the drops walk across the fluid bath. The walking regime arises only for a limited range of drop sizes and forcing conditions.

Couder's group has characterised the behaviour of drops bouncing on a fluid bath in terms of the drop diameter $D = 2r_0$ and dimensionless forcing acceleration $\Gamma = \gamma/g$.⁷⁻⁹ Protiere *et al.*⁷ conducted experiments with a viscosity-frequency combination of 50 cS-50 Hz and summarised their results in a regime diagram illustrating the droplet behaviour in the D - Γ plane. For low forcing accelerations, simple bouncing arises: the drop hits the bath once every driving period. Increasing the acceleration generally leads to a period-doubled bouncing state. For relatively small and large drops, a period doubling cascade may follow, culminating in chaotic bouncing or walking. For the larger drops, an intermittent regime can arise in which the drop changes from one bouncing state to another in an irregular fashion. For drops within a limited size range, there is a critical $\Gamma_w = \gamma_w/g$ above which they walk along the surface of the bath. The walking regime was previously thought to be associated exclusively with a fully period doubled bouncing state; however, more complex walking modes will be highlighted herein. A similar regime diagram was obtained for a 20 cS-80 Hz combination, the system being characterised in terms of the same four characteristic states.^{8,9} The theoretical rationale for the form of the regime diagrams was only recently developed,^{10,13} and will be built upon herein.

Gilet and Bush⁴ considered the motion of a drop on a vibrating soap film, and demonstrated that the film behaves like a linear spring with a spring constant proportional to the surface tension. They observed and rationalised a number of complex bouncing states, multiperiodicity (the existence of different bouncing states at identical system parameters), and period doubling transitions to chaos. Different bouncing states were denoted by (m, n) , where m/f represents the period of the bouncing mode, during which the drop contacts the surface n times. The dynamics of interest here, of droplets bouncing on a vibrating fluid bath, are significantly complicated by the influence of the fluid bath's inertia.

Molacek and Bush¹⁰ (henceforth MB1) examined droplets bouncing on a vibrating fluid bath, and detailed both experimentally and theoretically the dependence of the bouncing mode on the system parameters. They introduce the vibration number, $\Omega = 2\pi f \sqrt{\rho r_0^3 / \sigma}$, the relative magnitude

of the forcing frequency, and the drop's natural oscillation frequency, and summarised their results in regime diagrams that indicate the droplet behaviour in the Ω - Γ plane. They demonstrate that droplets of a given size can bounce at the lowest forcing amplitude when $\Omega \approx 0.65$, that is, when the drop is forced at its natural frequency. They noted different bouncing states with the same periodicity, which they denote by $(m, n)^i$, where the integer superscript i increases with the state's mean mechanical energy, specifically, the drop's combined kinetic and gravitational potential energy. In addition to identifying a number of previously unreported bouncing states, MB1 developed a theoretical model that rationalises the observed dynamics. The vertical interaction between the bouncing drop and the liquid bath during drop contact was described using a logarithmic spring model, which built upon their model of drop impact on a rigid substrate.²⁴

Molacek and Bush¹³ (henceforth MB2) extended their theoretical model in order to capture the dynamics of walking droplets. Specifically, their logarithmic spring model was supplemented by consideration of the wave field of the bath, which may destabilise the stationary bouncing states. While they rationalised the limited extent of the walking regime, they did not characterise the dependence of the walking style on the system parameters. Their model successfully rationalised the experimentally reported transitions from bouncing to walking states, as well as the dependence of the walking speed on the system parameters. They also noted the coexistence of different walking states at the same system parameters, and highlighted the predominance of the $(2, 1)^1$ and $(2, 1)^2$ modes. Finally, they reported a number of exotic walking states, including chaotic walkers and "limping" drops that walk with unequal steps, the focus of the present study.

The goal of the current study is to extend our knowledge of the bouncing drop dynamics by presenting the most detailed regime diagrams to date. In addition to reporting a number of new exotic bouncing and walking states, we extend the predictions of our theoretical model^{10,13} in order to rationalise our observations. In Sec. II, we describe our experimental set-up and present the experimentally obtained regime diagrams in which we identify the different walking and bouncing modes. We also examine the dependence of the walking speed on the bouncing mode. In Sec. III, we review our theoretical model and compare its predictions with our new experimental observations. Our results are summarised in Sec. IV.

II. EXPERIMENTS

In Figure 2, we present a schematic illustration of our experimental set-up. A circular fluid tray of diameter 76 mm and depth 16 mm is oscillated vertically in a sinusoidal manner with frequency f , amplitude A , and peak acceleration $\gamma = (2\pi f)^2 A$. The tray is vibrated by an industrial shaker mounted on a massive levelling platform, which rests beneath an optical table. The shaker is driven by a power amplifier controlled using a data acquisition system and custom software. We measure the acceleration using two piezoelectric accelerometers, and use a feedback loop to maintain a constant

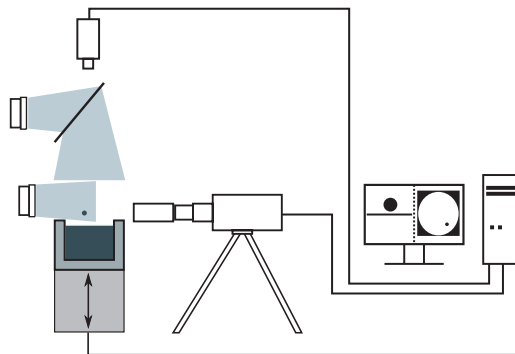


FIG. 2. Schematic illustration of the experimental set-up. The vibrating bath is illuminated by two LED lamps, and the drop motion recorded by two digital video cameras. The top view camera captures images at 17.5–20 frames per second, while the side view camera records at 4000 frames per second. The video processing is done on a computer.

vibration amplitude, corresponding to a tolerance of 0.01 g in vibrational acceleration amplitude. An air bearing carriage with a square cross section is mounted to a levelling platform to ensure that the vibratory motion lies strictly along a single vertical axis. The air bearing minimises lateral vibration introduced by the shaker, a technique developed for careful studies of vibrated granular layers.^{25–27} A thin coupling rod connects the shaker to the slider bar of the air bearing.

We use two different silicone oils, the first with kinematic viscosity $\nu = 20$ cS, density $\rho = 949$ kg/m³, and surface tension $\sigma = 20.6$ mN/m, and the second with $\nu = 50$ cS, $\rho = 965$ kg/m³, and $\sigma = 20.8$ mN/m. We identify the Faraday threshold γ_F for each combination of experimental parameters by gradually increasing the acceleration amplitude γ until standing waves with frequency $f/2$ form at the free surface. The precise value of γ_F depends on the vibration frequency, the depth, and viscosity of the oil. The dimensionless Faraday threshold is denoted by $\Gamma_F = \gamma_F/g$.

Oil drops are created by rapidly extracting a submerged needle from the fluid bulk.⁷ Of the droplets formed, we select those of radius r_0 between 0.20 mm and 0.51 mm. The undeformed drop radius r_0 is measured optically with a high-speed camera, recording at 4000 frames per second. The optical set-up results in a pixel density of 71–88 pixels per mm, leading to an uncertainty in drop radius of $\pm 1.5\%$. The horizontal motion of the drop is captured from above with a Machine Vision CCD camera and is tracked using particle-tracking software. We performed measurements for a single drop size by either increasing or decreasing the driving acceleration in a stepwise manner from some initial value of Γ , with typical step size $d\Gamma = 0.1\Gamma$. The entirety of the bouncing and walking regimes could thus be explored by varying γ between γ_B and γ_F .

Three different combinations of fluid viscosity and forcing frequency were investigated. A 20 cS silicone oil bath was forced at 70 and 80 Hz, and a 50 cS oil bath at 50 Hz. A full exploration of both walking and bouncing regions was conducted for the 20 cS-80 Hz combination, since this exhibited the richest behaviour. For the other two combinations, we focused on characterising the walking regimes. For each combination of oil viscosity and driving frequency, we present a regime diagram indicating the droplet bouncing behaviour in the Γ - Ω plane (Fig. 3). Spatiotemporal diagrams of selected bouncing and walking modes, deduced by transposing pixel-wide slices through the droplet's centerline obtained from successive frames, are presented in Figures 4–6. In Table I, a summary of the observed bouncing and walking modes is provided.

In the three regime diagrams reported in Fig. 3, the horizontal axis is the dimensionless forcing $\Gamma = \gamma/g$, and the vertical axis is the dimensionless vibration number Ω , a proxy for drop size. Individual markers correspond to experimental observations, with square and round markers denoting stationary bouncing and walking states, respectively. The colour of the marker denotes the observed bouncing or walking mode. We first describe the experimental results, and reserve the comparison with theoretical predictions for Sec. III.

A full exploration of both the bouncing and walking regimes for the 20 cS-80 Hz combination is shown in Fig. 3(a). For relatively weak forcing, $1.5 < \Gamma < 2.3$, the (2, 2) bouncing mode is dominant; however, a band of the (4, 4) mode (Fig. 4(a)) is also observed for vibration numbers $\Omega \lesssim 0.5$. As Γ is increased, additional $m = 4$ modes are observed. Specifically, the (4, 3) mode (Fig. 4(b)) arises in a region around $\Gamma \approx 2.6$ and $\Omega \approx 0.5$, and the (4, 2) mode (Fig. 4(c)) appears for almost all vibration numbers investigated, for $\Gamma > 3.3$, spanning both the bouncing and walking regimes. A region of (2, 1) bouncing modes extends from $\Gamma = 2.5$ up to Γ_F for vibration numbers between 0.6 and 1. This region crosses into the walking region, starting out in the low energy

TABLE I. The walking and bouncing modes observed for the three viscosity-frequency combinations examined. Modes in bold typeface are those for which an associated spatiotemporal diagram is included (see Figs. 4–6).

Fluid/frequency	Regime diagram	Bouncing and walking modes
20 cS-80 Hz	Fig. 3(a)	(2, 1) ¹ , (2, 1) ² , (2, 2), (4, 2) , (4, 3) , (4, 4) , chaotic; Fig. 4
50 cS-50 Hz	Fig. 3(b)	(2, 1)¹ , (2, 1)² , chaotic ; Fig. 5
20 cS-70 Hz	Fig. 3(c)	(2, 2) , (4, 3), (13, 10) , (2, 1) ¹ , (2, 1) ² , mixed mode , chaotic; Fig. 6

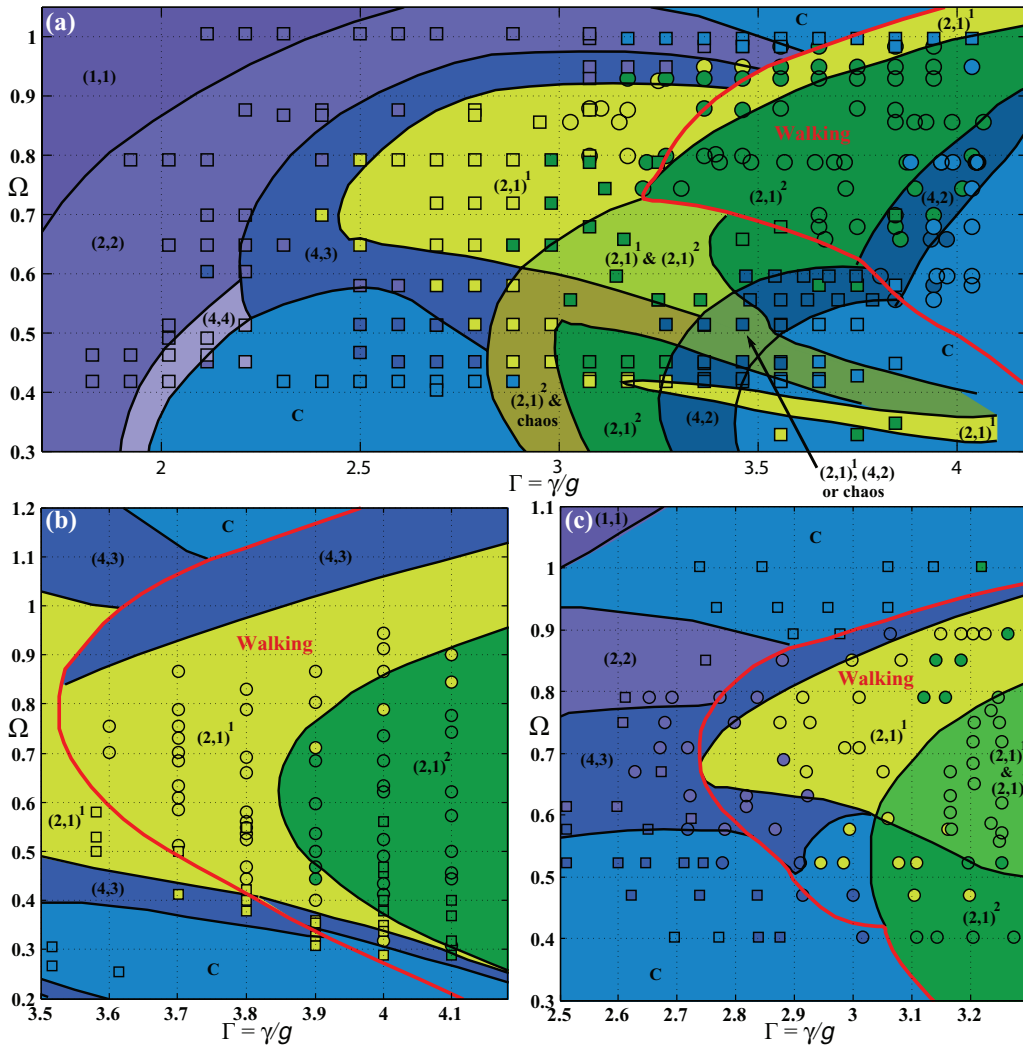


FIG. 3. Regime diagrams indicating the dependence of the droplet behaviour on the dimensionless driving acceleration, $\Gamma = \gamma/g$, and the vibration number, $\Omega = 2\pi f \sqrt{\rho r_0^3 / \sigma}$. (a) The 20 cS-80 Hz combination, for which $\Gamma_F = 4.22 \pm 0.05$. (b) The 50 cS-50 Hz combination, for which $\Gamma_F = 4.23 \pm 0.05$. (c) The 20 cS-70 Hz combination, for which $\Gamma_F = 3.33 \pm 0.05$. Coloured areas correspond to theoretical predictions, the solid red line denoting the theoretically predicted walking threshold. Experimental data are presented as square or round markers, with square markers denoting stationary bouncing states, round markers walking states, and their colour indicating the associated mode.

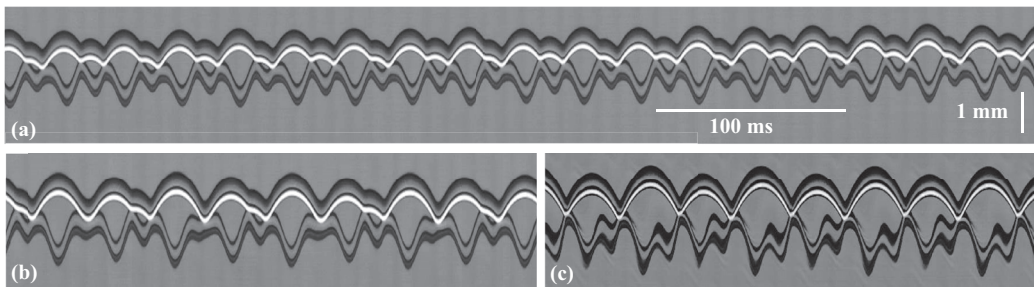


FIG. 4. Spatiotemporal diagrams of the bouncing modes observed for the 20 cS-80 Hz combination. (a) Bouncing mode (4, 4). $\Gamma = 2.3$, $\Omega = 0.45$. (b) Bouncing mode (4, 3). $\Gamma = 2.7$, $\Omega = 0.45$. (c) Bouncing mode (4, 2). $\Gamma = 3.5$, $\Omega = 0.42$.

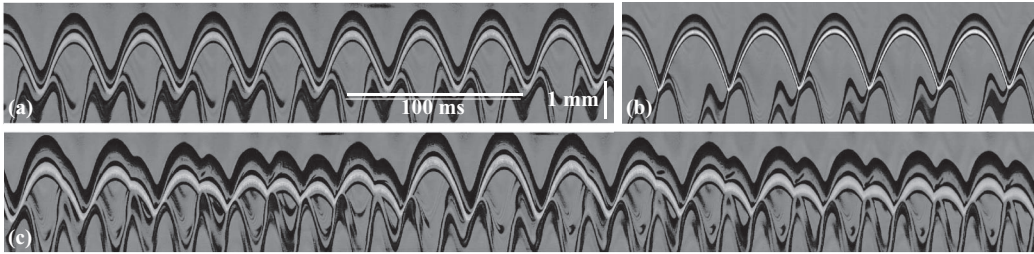


FIG. 5. Spatiotemporal diagrams of the modes observed for the 50 cS-50 Hz combination. (a) Walking mode $(2, 1)^1$. $\Gamma = 3.7$, $\Omega = 0.59$. (b) Walking mode $(2, 1)^2$. $\Gamma = 4.0$, $\Omega = 0.44$. (c) Chaotic bouncing with no apparent periodicity. $\Gamma = 4$, $\Omega = 0.94$.

$(2, 1)^1$ mode then transitioning into the high energy $(2, 1)^2$ mode as Γ is increased. The $(2, 1)$ bouncing states also arise for smaller drops, $\Omega \approx 0.4$ – 0.5 , along a band with Γ ranging from 2.9 to 3.3, at which a period doubling transition creates a $(4, 2)$ mode that eventually gives way to a chaotic region.

Three distinct regions of complex or chaotic motion are observed. One exists for drops bouncing with $2.3 < \Gamma < 3$ and $\Omega \approx 0.4$. Another arises near $3.5 < \Gamma < \Gamma_F$, $0.4 < \Omega < 0.8$ and spans the bouncing and walking regimes. For larger drops ($\Omega \approx 1$) there is a region of complex or chaotic behaviour stretching from the bouncing ($\Gamma \approx 3.1$) into the walking regime, and up to the Faraday threshold. Generally, near the Faraday threshold, the walking is observed to be chaotic, with only a relatively small window of periodic walking, for $0.8 < \Omega < 1$, above which chaotic bouncing is observed. For $\Omega \approx 1$, we observed stationary chaotic bouncing drops that, when perturbed with a submerged needle, could be induced to transition into a stable $(2, 1)$ walking mode.

The regime diagram deduced for the 50 cS-50 Hz combination is shown in Fig. 3(b). The observed modes were $(2, 1)^1$, $(2, 1)^2$, and chaotic bouncing, the form of which are presented in Fig. 5. Walking occurs only in the $(2, 1)^1$ and $(2, 1)^2$ modes, the horizontal drop speed being typically 2-3 times larger in the former than in the latter. The $(2, 1)^1$ mode (Fig. 5(a)) has a longer contact time than the higher energy $(2, 1)^2$ mode (Fig. 5(b)), for which a much more rapid shift in momentum occurs during impact. The impact phase relative to the vibrating bath is also different, as is the walking speed, which is approximately 4 times higher for the $(2, 1)^1$ mode. The drop is generally in the $(2, 1)^1$ mode near the walking threshold, but transitions to the $(2, 1)^2$ mode as Γ is increased, remaining in this state until the Faraday threshold is reached. Chaotic bouncing is observed for lower forcing and drop size (Fig. 5(c)).

The regime diagram for the 20 cS-70 Hz combination is shown in Fig. 3(c) and includes a number of exotic bouncing and walking modes. Outside the walking region, three bouncing modes are observed. For large ($\Omega \approx 1$) and small ($\Omega \approx 0.4$) vibration numbers, chaotic or highly complex bouncing states are evident. Fig. 6(a) shows a spatiotemporal evolution of a highly complex $(13, 10)$ mode. For intermediate Ω , $(4, 3)$ and $(2, 2)$ bouncing modes arise, the former being observed for drops with $\Omega \approx 0.4$ – 0.6 , and the latter for $\Omega \approx 0.6$ – 0.8 . Fig. 6(b) shows the spatiotemporal diagram of a drop in the $(2, 2)$ mode. We refer to these as limping drops, owing to their unequal step sizes. The $(4, 3)$ and $(2, 2)$ modes stretch into the walking region, where the $(2, 1)$ modes are dominant. Once again, the $(2, 1)^2$ mode is generally observed at lower Ω than the $(2, 1)^1$ mode.

Of particular interest is a region of “mixed states” for $\Gamma > 3.1$ and $0.55 < \Omega < 0.8$. Here the drops alternate between the low and high energy $(2, 1)$ modes, as shown in Fig. 6(c), where the evolution is from $(2, 1)^1$ to $(2, 1)^2$ to $(2, 1)^1$ to $(2, 1)^2$. While the heights of the jumps are roughly equal, the phase of impact shifts rapidly. In Fig. 7(a), the horizontal trajectory of a drop in the mixed state is shown. The shading of the trajectory reflects its local horizontal speed which fluctuates by a factor of 4 as it switches between the fast $(2, 1)^1$ mode and the slow $(2, 1)^2$ mode. Fig. 7(b) shows the velocity of the mixed mode as a function of arc-length. The variation of the velocity occurs over a distance of approximately one Faraday wavelength, resulting in a highly peaked power spectrum (Fig. 7(c)). We note that the mixed mode is generally quite robust; however, by perturbing the drop with the meniscus of a submerged pin or through spontaneous interaction with a boundary,

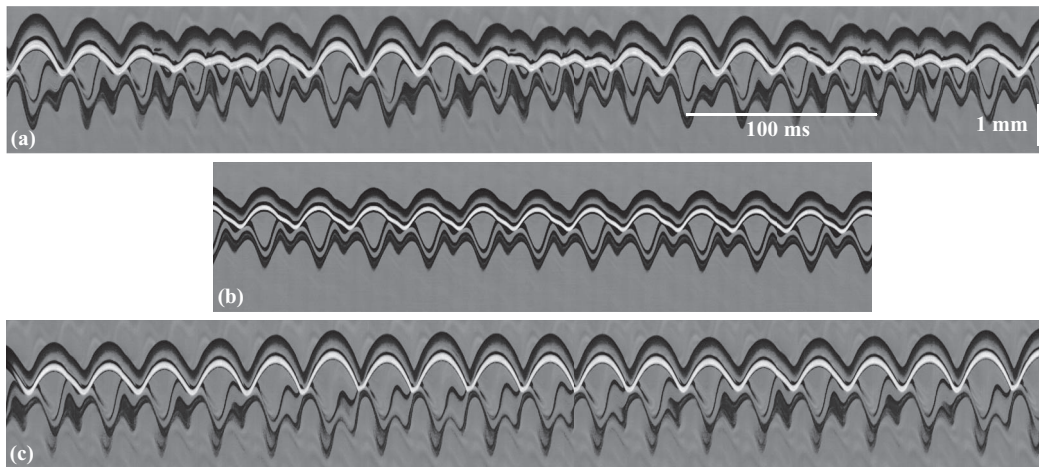


FIG. 6. Spatiotemporal diagrams of the modes observed for the 20 cS-70 Hz combination. (a) The exotic bouncing mode $(13, 10)$, highly complex periodic motion. $\Gamma = 3.3$, $\Omega = 0.97$. (b) The limping drop, a $(2, 2)$ walking mode. $\Gamma = 2$, $\Omega = 0.42$. (c) The mixed walking state, shown here evolving from $(2, 1)^1 \rightarrow (2, 1)^2 \rightarrow (2, 1)^1 \rightarrow (2, 1)^2$. $\Gamma = 3.4$, $\Omega = 0.72$.

it can be destabilised, causing the drop to shift into either the $(2, 1)^1$ or the $(2, 1)^2$ walking modes. Fig. 7(d) shows the trajectory of a mode switcher settling into the high energy $(2, 1)^2$ mode after being perturbed by an approach to the boundary at nearly normal incidence. We note that we might alternatively have denoted the mixed state by a purely periodic mode, $(24, 12)$; however, we find it

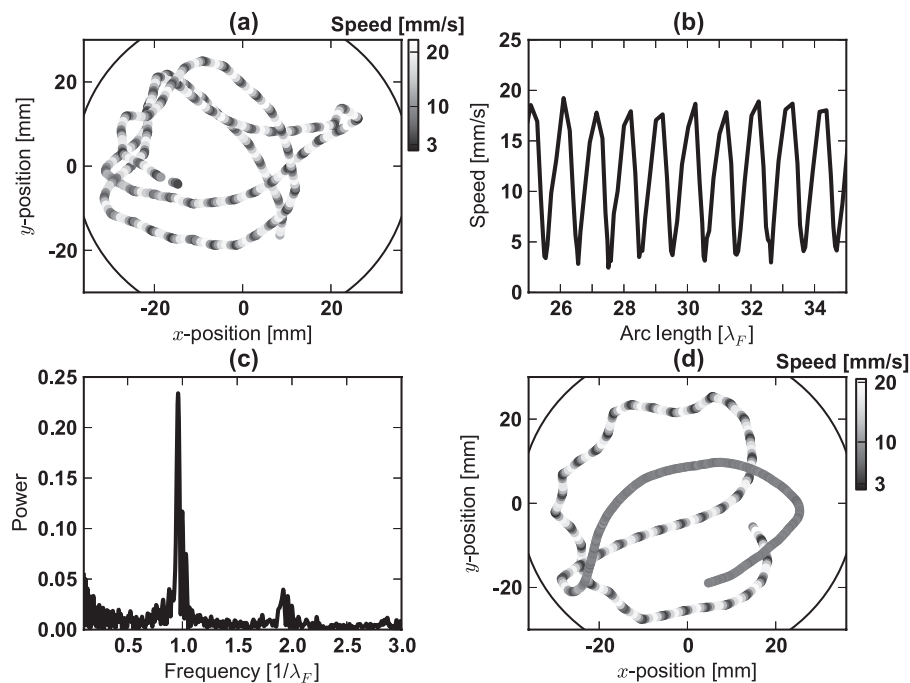


FIG. 7. Mixed state walkers observed with the 20 cS-70 Hz combination. $\Gamma = 3.4$, $\Omega = 0.72$. (a) The trajectory for a drop in the mixed state, shaded according to the speed. The circular bath domain is indicated. (b) The observed variation of walking speed with arc-length, as normalised by the Faraday wavelength. (c) A Fourier power spectrum of the normalised velocity fluctuations, which indicates that the mode-switching arises periodically, after the droplet has walked a distance of approximately $0.95\lambda_F$. (d) Trajectory of a mixed mode, shaded according to speed, that destabilises into a $(2, 1)^2$ walker after collision with the boundary near $(x, y) = (-25, -20)$ mm.

useful to distinguish between the two phases of its motion $((2, 1)^1$ and $(2, 1)^2$), in which its speed is markedly different.

III. THEORETICAL PREDICTIONS

In order to obtain theoretical predictions for the dependence of the bouncing behaviour on the system parameters, we adopted the model presented in MB1 and MB2. There, it was shown that the vertical drop motion is governed by

$$-mg^*(t) = m\ddot{z} \quad \text{in free flight } (\mathcal{Z} \geq 0 \text{ or } F_N \leq 0), \quad (2)$$

$$-mg^*(t) = \left(1 + \frac{c_3}{\ln^2 \left| \frac{c_1 r_0}{\mathcal{Z}} \right|}\right) m\ddot{z} + \frac{4\pi\mu r_0 c_2(v)}{3 \ln \left| \frac{c_1 r_0}{\mathcal{Z}} \right|} \dot{\mathcal{Z}} + \frac{2\pi\sigma\mathcal{Z}}{\ln \left| \frac{c_1 r_0}{\mathcal{Z}} \right|} \quad \text{during contact},$$

where m is the drop mass, z is its center of mass, and $\mathcal{Z} = z - h$ is the height of the drop above the bath surface. During free flight, the drop responds only to gravity. During impact, $F_N(t) = m\ddot{z} + mg^*(t)$ is the normal component of the reaction force acting on the drop. The constants used here, $c_1 = 2$, $c_3 = 1.4$, $c_2 = 12.5$ for 20 cS oil and $c_2 = 7.5$ for 50 cS oil, were deduced in MB1 by matching with experimental measurements of the normal and tangential coefficients of restitution. To consider one-dimensional horizontal drop motion, we write $h = h(x, t)$ as the total height of the standing waves in the bath frame of reference. $h(x, t)$ can be expressed as the sum of contributions from all previous impacts:

$$h(x, t) = \sum_{n=1}^N h_0(x, x_n, t, t_n). \quad (3)$$

The contribution $h_0(x, x_n, t, t_n)$, resulting from a single drop impact at $(x, t) = (x_n, t_n)$, can be approximated, in the long-time limit, by a standing wave decaying exponentially in time with a spatial profile prescribed by a zeroth order Bessel function of the first kind, $J_0(x)$:

$$h_0(x, x_n, t, t_n) \approx J_0(k_F(x - x_n)) \sqrt{\frac{2}{\pi}} \frac{k_F r_0}{3k_F^2 r_0^2 + \mathcal{B}o} \frac{r_0 k_F^2 \mu_{eff}^{1/2} \cos(\pi f t)}{\sigma \sqrt{t - t_n}} \times \exp\left\{(\Gamma/\Gamma_F - 1) \frac{t - t_n}{T_d}\right\} \int F_N(t') \sin(\pi f t') dt'. \quad (4)$$

Here, $\mathcal{B}o = \rho g r_0^2 / \sigma$ is the Bond number, and T_d is the characteristic decay time of the unforced waves, which depends on the fluid viscosity and the critical wavenumber. μ_{eff} is a phenomenological viscosity required to ensure that the decay rate of the waves matches that in a fully analytical model (MB2, Appendix A.1). The integral of the reaction force, $F_N(t)$, is carried out over the duration of contact.

In order to increase computational speed, the number of previous impacts stored is kept to a manageable size by discarding those whose standing wave amplitude has decayed sufficiently (below 0.1% of its initial value). Since the contact takes place over a finite length of time, x_n and t_n are taken as the weighted averages of x and t over the contact time t_c , defined as the interval during which the vertical reaction force $F_N(t)$ on the drop is positive:

$$x_n = \frac{\int_{t_c} F_N(t') x(t') dt'}{\int_{t_c} F_N(t') dt'}, \quad t_n = \frac{\int_{t_c} F_N(t') t' dt'}{\int_{t_c} F_N(t') dt'}. \quad (5)$$

The horizontal dynamics is governed by

$$m\ddot{x} + D(t)\dot{x} = -\frac{\partial h(x, t)}{\partial x} \cdot F_N(t), \quad (6)$$

where

$$D(t) = 0.17 \frac{\sqrt{\rho r_0}}{\sigma} F_N(t) + 6\pi r_0 \mu_a \left(1 + \frac{g r_0}{12} v_a f\right) \quad (7)$$

is the total instantaneous drag coefficient. The subscript a denotes air. The first term represents the momentum drag induced during impact and the second term represents the aerodynamic drag induced during flight. The term on the right-hand side of Eq. (6) is the propulsive wave force applied during contact, which is well approximated by the tangential component of the total reaction force.

The system of Eqs. (2)–(6) was solved numerically, with time step $0.05\sqrt{\rho r_0^3/\sigma}$ during contact, the duration of which was typically at least $4\sqrt{\rho r_0^3/\sigma}$. We followed a procedure akin to that adopted to obtain the experimental data reported in Fig. 3; specifically, we scan a wide range of Ω ($0.2 \leq \Omega \leq 1.2$), with increments of $d\Omega = 0.005$. For each Ω value, we start at a value of Γ close to the Faraday threshold, specifically $\Gamma = 0.99\Gamma_F$, then decrease Γ in small increments until reaching some pre-defined lower limit. We shall refer to one such sweep of Γ as a *run*. The bath is taken to be initially quiescent, $h(x, 0) = 0$. We performed several runs, starting each with different initial conditions on the drop position $z(0)$ and speed $\dot{z}(0)$, so as to increase the likelihood of discovering all the possible bouncing modes in case of the coexistence of multiple modes. Usually, this meant setting $z(0) = 0$ and varying $\dot{z}(0)$ between -0.3 and 0.3 .

For relatively large drops close to the Faraday threshold, as in our experiments, both walking and bouncing states may arise at identical system parameters. To ensure resolution of the walking solution, the initial horizontal speed was set to a value higher than the equilibrium speed. Then, for each run, we slowly decreased Γ in steps $d\Gamma = 0.001\Gamma_F$, at each step waiting for the walking speed to converge, specifically until the difference between the average walking speed at successive impacts drops below 0.1%:

$$0.999 < \left| \frac{\bar{v}_t}{\bar{v}} \right| < 1.001, \quad (8)$$

where \bar{v} and \bar{v}_t are the average horizontal drop speed up to the time of the penultimate and last impacts, respectively.

At each Γ value, we recorded the period of vertical motion and number of contacts per period, which yielded the (m, n) mode number. We also recorded the average contact time \bar{T}_C , the total contact time per period of vertical motion divided by the number of contacts n . This allowed us to differentiate between different energy levels, as the high energy modes had $\bar{T}_C < 5\sqrt{\rho r_0^3/\sigma}$ (typically, $\bar{T}_C \approx 3.5\sqrt{\rho r_0^3/\sigma}$), while the low energy modes had $\bar{T}_C > 5\sqrt{\rho r_0^3/\sigma}$ (typically, $\bar{T}_C \approx 8\sqrt{\rho r_0^3/\sigma}$). When the forcing is decreased below a critical value Γ_W , the walking speed drops to 0. The equations of motion can then be simplified considerably, as (6) is identically 0, and $J_0(k_C(x - x_n)) = 1$ in (4). Assimilation of the data obtained by this procedure yielded our theoretical regime diagrams (Fig. 3). Numerically computed vertical bouncing modes with corresponding surface displacements are provided in MB1 (Figures 16–18) and MB2 (Figure 16).

The solid coloured regions of Figs. 3(a)–3(c) indicate the theoretically predicted bouncing modes. The red line indicates the predicted walking threshold. For the 20 cS-80 Hz combination (Fig. 3(a)) several modes are found to exist where predicted, including the observed (2, 1), (2, 2), (4, 4), (4, 2), and chaotic modes. The experimental walking threshold for large and small vibration numbers ($\Omega < 0.7$ and $\Omega > 0.9$) coincides with the theoretical predictions; however, for drops of intermediate size, the agreement is less convincing. The (4, 3) bouncing mode is experimentally observed for smaller drop sizes than predicted, and the experimental (2, 1)¹ bouncing region extends further into the theoretical (4, 3), (2, 1)², and chaotic regions than predicted. The model does capture the observed (2, 1)¹-branch cutting across several other regions near $\Gamma \approx 3$ –4 and $\Omega < 0.6$.

For the 50 cS-50 Hz combination (Fig. 3(b)), the observed and predicted (2, 1)¹ and (2, 1)² modes coincide convincingly, and the theoretical and experimental walking thresholds also match. Furthermore, chaotic bouncers were observed inside the theoretically predicted chaotic region. The (4, 3) walking regime was not observed experimentally, but might have been had larger drops been examined.

For the 20 cS-70 Hz regime diagram (Fig. 3(c)), the observed chaotic region for large drops ($\Omega \approx 1$) coincides with that predicted. For smaller drops ($\Omega \approx 0.4$ –0.6), the observed (4, 3) mode

is offset relative to that predicted, as was the case in the experiments at 20 cS-80 Hz (Fig. 3(a)). The (2, 2) bouncing mode is also observed at slightly lower vibration numbers than predicted. The observed high and low energy (2, 1) modes do not coincide precisely with the theory within the walking region, but the walking threshold is generally well-predicted. The mixed mode region found experimentally corresponds closely to the theoretically predicted region of coexistence of the (2, 1)¹ and (2, 1)² modes. We note that a true mixed mode, characterised by a stable periodic shift between the low and high energy (2, 1) modes, has not yet been observed theoretically.

Finally, we note that in our experiments the threshold between bouncing states generally depends on whether it was approached from above or below. Specifically, by increasing and decreasing Γ across a regime boundary, the Γ threshold between states has a characteristic uncertainty of $\Delta\Gamma \approx 0.1$. This hysteresis, which may reflect the existence of prolonged transient behaviour, provides some rationale for the relatively small discrepancy between theory and experiment. We note that significantly less hysteresis was apparent in the simulations, which could be simply extended beyond any transient behaviour.

IV. CONCLUSION

We have conducted a combined experimental and theoretical study of drops bouncing on a vibrating fluid bath, and focused on the parameter regime of interest to workers in hydrodynamic quantum analogs. By comparing our experimental results with the theory developed in MB1 and MB2, we have extended the current knowledge of the bouncing droplet system. We have enumerated the myriad styles in which drops can bounce and walk, and presented, in Fig. 3, the most detailed experimental and theoretical regime diagrams to date. Particular attention has been given to elucidating the rich and varied dynamics within the walking regime, an understanding of which will assist in rationalising the quantum-like behaviour of walking drops. Finally, we have highlighted a mixed state, in which the walking drop shifts between two distinct modes, a state that may prove valuable in expanding the range of hydrodynamic quantum analog systems.

ACKNOWLEDGMENTS

The authors gratefully acknowledge the financial support of the National Science Foundation (NSF) through Grant No. CBET-0966452. Ø.W.-W. thanks The Danish National Advanced Technology Foundation for financial support through the NanoPlast project. D.M.H. thanks the NSF Graduate Research Fellowship Program for financial support.

- ¹J. Walker, "Drops of liquid can be made to float on the liquid. What enables them to do so?," *Amateur Scientist, Sci. Am.* **238**, 151–158 (1978).
- ²Y. Couder, E. Fort, C.-H. Gautier, and A. Boudaoud, "From bouncing to floating: Noncoalescence of drops on a fluid bath," *Phys. Rev. Lett.* **94**, 177801 (2005).
- ³T. Gilet, D. Terwagne, N. Vandewalle, and S. Dorbolo, "Dynamics of a bouncing droplet onto a vertically vibrated interface," *Phys. Rev. Lett.* **100**, 167802 (2008).
- ⁴T. Gilet and J. W. M. Bush, "The fluid trampoline: Droplets bouncing on a soap film," *J. Fluid Mech.* **625**, 167–203 (2009).
- ⁵T. Gilet and J. W. M. Bush, "Chaotic bouncing of a droplet on a soap film," *Phys. Rev. Lett.* **102**, 014501-1–014501-4 (2009).
- ⁶Y. Couder, S. Protiere, E. Fort, and A. Boudaoud, "Dynamical phenomena: Walking and orbiting droplets," *Nature* **437**, 208 (2005).
- ⁷S. Protiere, A. Boudaoud, and Y. Couder, "Particle-wave association on a fluid interface," *J. Fluid Mech.* **554**, 85–108 (2006).
- ⁸A. Eddi, D. Terwagne, E. Fort, and Y. Couder, "Wave propelled ratchets and drifting rafts," *Europhys. Lett.* **82**, 44001 (2008).
- ⁹A. Eddi, E. Sultan, J. Moukhtar, E. Fort, M. Rossi, and Y. Couder, "Information stored in Faraday waves: the origin of a path memory," *J. Fluid Mech.* **674**, 433 (2011).
- ¹⁰J. Molacek and J. W. M. Bush, "Drops bouncing on a vibrating bath," *J. Fluid Mech.* **727**, 582–611 (2013).
- ¹¹L. de Broglie, "Interpretation of quantum mechanics by the double solution theory," *Ann. Fond. Louis Broglie* **12**(4), 1–23 (1987).
- ¹²Y. Couder and E. Fort, "Probabilities and trajectories in a classical wave-particle duality," *J. Phys.: Conf. Ser.* **361**, 012001 (2012).

- ¹³J. Moláček and J. W. M. Bush, “Drops walking on a vibrating bath: towards a hydrodynamic pilot-wave theory,” *J. Fluid Mech.* **727**, 612–647 (2013).
- ¹⁴J. W. M. Bush, “Quantum mechanics writ large,” *Proc. Natl. Acad. Sci. U.S.A.* **107**(41), 17455–17456 (2010).
- ¹⁵A. Eddi, A. Decelle, E. Fort, and Y. Couder, “Archimedean lattices in the bound states of wave interacting particles,” *Europhys. Lett.* **87**, 56002 (2009).
- ¹⁶A. Eddi, A. Boudaoud, and Y. Couder, “Oscillating instability in bouncing droplet crystals,” *Europhys. Lett.* **94**, 20004 (2011).
- ¹⁷Y. Couder and E. Fort, “Single-particle diffraction and interference at a macroscopic scale,” *Phys. Rev. Lett.* **97**, 154101 (2006).
- ¹⁸E. Fort, A. Eddi, A. Boudaoud, J. Moukhtar, and Y. Couder, “Path-memory induced quantization of classical orbits,” *Proc. Natl. Acad. Sci. U.S.A.* **107**(41), 17515–17520 (2010).
- ¹⁹A. Eddi, J. Moukhtar, S. Perrard, E. Fort, and Y. Couder, “Level splitting at macroscopic scale,” *Phys. Rev. Lett.* **108**, 264503 (2012).
- ²⁰A. Eddi, E. Fort, F. Moisy, and Y. Couder, “Unpredictable tunneling of a classical wave-particle association,” *Phys. Rev. Lett.* **102**, 240401 (2009).
- ²¹D. M. Harris, J. Moukhtar, E. Fort, Y. Couder, and J. W. M. Bush, “Wavelike statistics from pilot-wave dynamics in a circular corral,” *Phys. Rev. E* **88**, 011001 (2013).
- ²²S. Douady, “Experimental study of the Faraday instability,” *J. Fluid Mech.* **221**, 383–409 (1990).
- ²³T. B. Benjamin and F. Ursell, “The stability of the plane free surface of a liquid in vertical periodic motion,” *Proc. R. Soc. London, Ser. A* **225**(1163), 505–515 (1954).
- ²⁴J. Moláček and J. W. M. Bush, “A quasi-static model of drop impact,” *Phys. Fluids* **24**, 127103-1–127103-16 (2012).
- ²⁵P. M. Reis, R. A. Ingale, and M. D. Shattuck, “Forcing independent velocity distributions in an experimental granular fluid,” *Phys. Rev. E* **75**, 051311 (2007).
- ²⁶D. I. Goldman, “Pattern formation and fluidization in vibrated granular layers, and grain dynamics and jamming in a water fluidized bed,” Ph.D. thesis, University of Texas at Austin (2002).
- ²⁷J. R. de Bruyn, B. C. Lewis, M. D. Shattuck, and H. L. Swinney, “Spiral patterns in oscillated granular layers,” *Phys. Rev. E* **63**, 041305 (2001).